JOM
https://doi.org/10.1007/s11837-019-03635-0

Nitrogen Incorporation Induced Soft-to-Hard Transition Observed in the Mechanical Properties of Amorphous Niobium Oxide Films

C. OROZCO,[1] O.R. NUNEZ,[1] N.R. MURPHY,[2] J.G. JONES,[2] and C.V. RAMANA[1,3]

1.—Center for Advanced Materials Research (CMR), University of Texas at El Paso, El Paso, TX 79968, USA. 2.—Materials and Manufacturing Directorate (RX), Wright-Patterson Air Force Base (WPAFB), 3005 Hobson Way, Dayton, OH 45433, USA. 3.—e-mail: rvchintalapalle@utep.edu

The article covers the nitrogen incorporation induced transformation of mechanical behavior of the amorphous Nb-oxide films. Niobium oxynitride (Nb-O-N) films were sputter-deposited using a metallic Nb target in the presence of oxygen and nitrogen. The nitrogen concentration in the Nb-O-N films was varied by adjusting the nitrogen gas flow rate from 0 sccm to 10 sccm while keeping total gas flow (nitrogen + oxygen + argon) constant at 30 sccm. The surface and interface chemical characterization of the samples indicate that, with increasing the nitrogen content, the corresponding mechanical characteristics, namely, hardness (H) and elastic modulus (E), increase from $\sim$ 5 GPa to 15 GPa and 115 GPa to 135 GPa, respectively. The trend observed in H and E values correlates with Nb-O and Nb-N bond formation in Nb-O-N as evidenced in chemical analyses made using x-ray photoelectron spectroscopy. The chemical composition measurements indicate that nitrogen incorporation proceeds with a decrease in relative oxygen content in Nb-O-N films, where the ability to withstand mechanical deformation is enhanced. A correlation between the processing conditions, nitrogen content, and physical/mechanical properties in Nb-O-N films is established.

INTRODUCTION

Niobium oxide (Nb_2O_5) exhibits interesting physical, chemical, electrical, optical, and optoelectronic properties, which are quite useful for utilization in energy conversion and storage devices and chemical sensors.[1–4] The excellent optical and electronic properties, along with good chemical stability, have led to several studies exploring Nb_2O_5 films for use in solar cell technology.[5,6] Nb_2O_5 also displays electrochromic properties, which are useful for its utilization in energy-efficient windows, electronic displays, and sustainable energy applications.[7–10] In addition, most recently, significant efforts were made in the literature to realize the potential applications of thin film and nanostructured Nb_2O_5 in batteries and other electronic devices such as memristors and chemical sensors. In addition to Nb-oxides, niobium nitrides (Nb-N) also have shown to exhibit excellent mechanical characteristics such as high hardness values, melting point, and coefficient of friction leading to their use as protective coatings and diffusion barriers.[11–13] Additionally, superconducting properties of Nb-N films were demonstrated for application in contact devices.[14] Recently, modification or tuning of the physical, chemical, and electronic properties to obtain controlled phase, stability, and morphology of Nb_2O_5 has been gaining importance. Specifically, anion or cation doping of Nb_2O_5 has the benefit of allowing the formation of a material that can simultaneously exhibit the characteristics of both an oxide and a nitride. By forming an Nb-oxynitride (Nb-O-N), it is not only possible to tune the desired optical properties but also to combine the attractive properties of Nb-oxides with the mechanical and electronic properties of Nb-nitrides. In this context, the

C. Orozco and O.R. Nunez have been contributed equally contributed to this work.

Published online: 12 July 2019

present work was focused on understanding the effect of nitrogen incorporation on the surface and interface characteristics and their influence on the mechanical behavior of Nb-O-N films made by reactive deposition.

A wide variety of physical and chemical deposition methods have been employed to fabricate thin films and coatings of Nb-oxides, Nb-nitrides, and Nb-oxynitrides.[15–30] Early attempts to fabricate Nb-O-N films involved methods of oxidizing Nb-nitride.[15,16] Later attempts were focused on the fabrication of Nb-O-N using physical vapor deposition[17] and rapid thermal processing.[18] Bekermann et al.[19] fabricated Nb-O-N thin films by using metalorganic chemical vapor deposition (MOCVD) in order to improve step coverage of complex substrate geometries. Nb-O-N thin films have been directly used in several applications to improve overall mechanical and optical behavior. Nb-O-N films were explored for their application as Josephson junctions[15,16,19] and optical waveguides.[20] In the form of a bulk material, Nb-O-N has been used in catalysis for different chemical reactions.[21,22] In addition, Nb-O-N thin films have been applied in multilayered systems for use in biomedical applications[17] and as a top layer to better resist wear and corrosion.[23] Several works by Fenker et al. investigated the influence of several key parameters on the mechanical, corrosion resistance, and optical properties of Nb-O-N. Along with the chemical composition, the film's structure[24] and method of deposition[25] were investigated to provide insight into their effect on the mechanical and corrosion behavior of Nb-O-N.

Our interest in Nb-based oxides and oxynitrides is primarily due to their variability in structural and optical properties, which can be readily utilized in optical and photonic devices.[31] In particular, the design and development of optical filters, antireflection coatings, and photo-electrochemical cells, where single or multilayered optical coatings play a key role, is the impetus to consider thin film fabrication and characterization of Nb oxides and oxynitrides. However, in these applications, understanding the surface/interface chemistry and control over the phase and composition is the key to tailor the materials' performance. Additionally, the structure, mechanical integrity, and optical properties are the most important parameters that dictate the device applications. As such, the present work was performed on the Nb-O-N thin films deposited by DC sputtering to understand the surface and interface science as a function of nitrogen incorporation. Specifically, efforts were directed toward the amorphous Nb-O-N films, which can be useful for integration into antireflection coatings and optical filters in addition to a direct comparison with the intrinsic and doped multivariant Nb-oxide materials. The primary objective of this work is to understand the kinetics of nitrogen incorporation, the nitrogen-incorporation induced changes in the surface/interface chemistry, and the associated effects on physical and mechanical characteristics. The effect of relative changes in the composition and Nb-O/Nb-N bonds on the mechanical properties and nitrogen-incorporation induced soft-to-hard transition in the amorphous Nb-O-N films are discussed in this article.

EXPERIMENTAL DETAILS

Fabrication

Direct current (DC) sputtering was utilized to fabricate Nb-O-N thin films. The films were deposited onto silicon Si (100) and quartz substrates. A 50-mm niobium (Nb) target was employed to facilitate reactive sputtering of the thin films. The vacuum chamber, described in detail elsewhere,[31] was evacuated to a base pressure of $\sim 2.67 \times 10^{-11}$ kPa. Plasma ignition was accomplished by supplying 200 W of power, from an Advanced Energy MDX 500 DC power supply, to the Nb-target with the sputtering source positioned 80 mm from the substrate. A reactive gas mixture comprising oxygen and nitrogen was used in conjunction with argon for the reactive deposition of Nb-O-N films. The total gas flow (nitrogen + oxygen + argon) was maintained constant at 30 sccm. The flow of argon was kept constant at 20 sccm, and the pressure was set at 2.67×10^{-4} kPa by adjusting a VAT automated gate valve resulting in a constant pumping speed of 135 L/s. The combined reactive gas mixture flow for oxygen and nitrogen was adjusted to a total of 10 sccm, and under the prescribed experimental conditions, the reactive gas mixture partial pressure remained at 1.1×10^{-4} kPa prior to plasma ignition. The reactive gas flow mixture was balanced with oxygen to a total of 10 sccm by carefully varying the nitrogen flow. More specifically, while keeping the total reactive gas (nitrogen + oxygen) flow always at 10 sccm, the gas flow of nitrogen was varied in steps of 2 sccm. Thus, oxygen gas flow was balanced to make up the total flow of 10 sccm. The resulting working pressure, which was maintained constant for all the depositions made, was held at 3.73×10^{-4} kPa. Deposition of the films was performed at room temperature (25°C) and for a time period of 10 min for each sample. A summary of the conditions used for depositing the Nb-O-N films is presented in Table I.

Characterization

X-Ray Diffraction (XRD)

X-ray diffraction (XRD) measurements were performed on the samples deposited onto Si(100) by a Bruker D8 Advance x-ray diffractometer. XRD measurements were performed ex situ at room temperature and as a function of nitrogen flow rate. Since the films were potentially thin enough to expect interaction form the substrate material,

Table I. Reactive sputtering parameters employed for the deposition of Nb-O-N films

Physical parameter	Set value
Base pressure	$\sim 3.67 \times 10^{-8}$ kPa
Sputtering power	200 W
Processing gases	Ar, N_2, O_2
Substrates	Silicon and quartz
Deposition temperature	Room temperature (25°C)
Target-to-substrate distance	8 cm
Total gas flow	30 sccm (constant)
Ar gas flow	20 sccm (constant)
N_2 gas flow	0–10 sccm (variable)
O_2 gas flow	0–10 sccm (balanced)
Working pressure	3.73×10^{-4} kPa
Pumping speed	135 L/s
Deposition time	10 min

grazing incidence x-ray diffraction (GIXRD) was used to avoid measuring the substrate. GIXRD patterns were recorded with Cu Kα radiation (λ = 1.54056 Å) at a voltage of 40 kV to generate the x-rays. The x-ray beam was fixed at a grazing incidence of 2°, and the "detector scan" mode was used to perform scanning in the 2θ range of 20° to 60°. The step size and scan speed utilized for the scans were 0.05° (2θ) and 5°/min, respectively.

X-Ray Photoelectron Spectroscopy (XPS)

The chemical composition of Nb-O-N films was determined by x-ray photoelectron spectroscopy (XPS). The composition and chemistry, including quantification of nitrogen uptake, was determined using XPS. Both XPS survey and high-energy resolution scans were obtained using a Physical Electronics 5700 equipped with a monochromatic Al Kα (1486.6 eV) x-ray source. Compositional analysis was performed using survey scans at an analyzer pass energy of 187.85 eV in a binding energy range spanning 0 eV to 1200 eV, while a lower analyzer pass energy of 29.35 eV was used for high-energy resolution measurements to examine the chemistry of the films. All spectra were charge calibrated with respect to the adventitious carbon 1-s transition at a binding energy of 284.6 eV. High-energy resolution scans of were fit with 30% Gaussian 70% Lorentzian line shapes following Shirley background subtraction. XPS data were processed and fit using the CasaXPS 2.3.16 software package.[32] Core-level transitions analyzed in this study include Nb 3*d*, C 1*s*, O 1*s*, and N 1*s*. Note that particulate emphasis is placed on the response of the Nb 3*d* and N 1*s* transitions. To limit the degrees of freedom present in the fits, the spacing between Nb $3d_{5/2-}$ and $3d_{3/2}$ transitions was constrained at 2.8 eV with an area ratio of 3:2. Inert gas sputtering was used for the removal of contamination layers resulting from air exposure using Ar^+ with a beam energy of 4 keV and a raster size of 3 mm by 3 mm using a cycle time of 0.3 min.

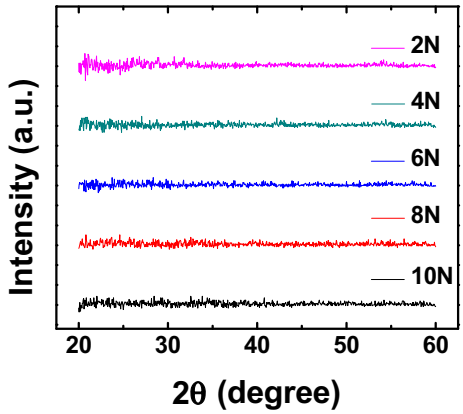

Fig. 1. XRD patterns of Nb-O-N films. The diffuse patterns without any peaks indicate the amorphous nature of all the Nb-O-N films.

Nano-mechanical Characterization

Nano-indentation was performed on samples deposited on Si(100) substrates to obtain the mechanical characteristics of Nb-O-N films. Using a Hysitron TI 750 TriboIndenter, the hardness (H) and elastic modulus (E_r) were determined using the technique outlined by Oliver and Pharr.[33] Load control nano-indentation was performed with a Berkovich tip with a 396-nm radius of curvature. A maximum load of 200 μN was used to penetrate depths of 10 nm to 20 nm in order to avoid contribution from the substrate material. Indentation was performed at 12 separate points on each sample, and the results averaged, to improve the accuracy of the results.[33,34] The load versus displacement curves and indentation patterns are correlated with the original probe calibration sheet that is supplied with each probe. The elastic modulus (E_r) can be calculated by finding the stiffness (S) of the film using the relation:[33]

$$E_r = \frac{\sqrt{\pi}}{2}\frac{S}{\sqrt{A}} \quad (1)$$

where A is defined as the area of contact at peak load. To find the hardness, the same value for the area of contact is used along with the maximum load (P_{max}) in:

$$H = \frac{P_{max}}{A} \quad (2)$$

The final statistical average of the H and E_r values calculated were considered to further assess the material's mechanical behavior as a function of deposition conditions of Nb-O-N films.

RESULTS AND DISCUSSION

GIXRD patterns for Nb-O-N thin films, as a function of nitrogen flow rate, are presented in Fig. 1. The GIXRD patterns reveal that the films

are amorphous in nature as there are no diffraction peaks to indicate crystalline growth. Since no additional thermal or electrical energy was supplied in the form of substrate heating and voltage bias, respectively, the films did not have sufficient energy to promote phase formation. Similar results have been observed for Nb-O-N thin films grown without additional supplied energy.[24,28,30] Furthermore, the formation of amorphous of Nb-O-N films due to lack of either thermal or electrical energy is in agreement with several other reports, where an amorphous structure is noted for Nb-oxides, W-oxides, W-O-N, and W-Ti mixed oxide thin films.[35–39]

X-ray photoelectron spectroscopy data were used to obtain the chemical composition and chemical state of the elements present in the Nb-O-N films. The XPS survey spectra of Nb-O-N films deposited under variable nitrogen flow rates are shown in Fig. 2. As noted in Fig. 2, the main constituents of the films are Nb, O, N, and C. The carbon peak in the XPS spectra is due to adventitious carbon from exposure to air after fabrication, before being placed in the XPS system. Therefore, the spectra is calibrated to the C 1*s* peak at a binding energy (BE) of 284.6 eV. However, sputtering the superficial layer with Ar^+ ions fully eliminated the C 1*s* peak in the survey scans (not shown), which is a clear indication that the carbon is a result of adsorbed species on the film surface due to air exposure from the transportation of the films from the sputtering chamber to the analysis chamber. Interestingly, the N 1*s* peak is only detected for a nitrogen flow rate of ≥ 6 sccm. The evolution of N 1*s* peak in survey spectra is shown with marked dotted lines (Fig. 2). This observation is not surprising since, like other niobium oxynitride films[24,25,29] and similar to nitrogen doped oxides,[38,39] nitrogen incorporation does not take place right away or until the required nitrogen flow rates and partial pressures are achieved. Thus, the XPS survey results displayed in Fig. 2 indicate that nitrogen incorporation does not take place in the Nb-oxide samples deposited with ≤ 6 sccm of nitrogen flow. A more detailed account of the chemical state analysis of Nb, N, and O has been performed considering the high-resolution scans of core level XPS.

The core-level XPS data of Nb and N are presented in Figs. 3 and 4, respectively, where the binding energy (BE) position and evolution of the Nb 3*d* and N 1*s* peaks as a function of nitrogen flow rate are presented. The Nb 3*d* exhibits the characteristic doublet, due to spin–orbit splitting, namely the Nb $3d_{5/2}$ and Nb $3d_{3/2}$ peaks at ∼ 207.18 eV and ∼ 209.90 eV, respectively. The binding energies of the 3*d* transitions, along with the spin–orbit splitting (ΔE(Nb 3*d*)) of 2.72 eV, characterizes the Nb ions in their highest oxidation state (Nb^{5+}) corresponding to the formation of Nb_2O_5.[19,40] It can be seen that no significant changes are observed with increasing nitrogen flow up to 6 sccm; at which point, there appears an additional component is evolved. For nitrogen gas flow rates < 6 sccm, the BE of the $3d_{5/2}$ and $3d_{3/2}$ peaks and ΔE(Nb 3*d*) were still within the range commonly reported for the Nb^{5+} valence state corresponding to Nb_2O_5. However, as the nitrogen flow increases above 6 sccm, an additional component evolves at a lower binding energy with Nb $3d_{5/2}$ and $3d_{3/2}$ peaks at binding

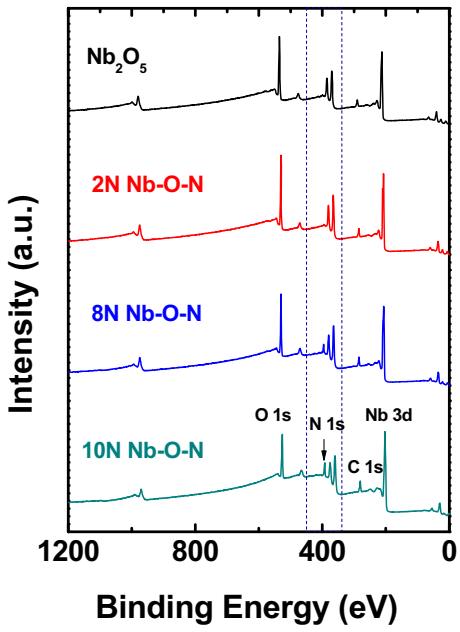

Fig. 2. XPS survey spectra of Nb-O-N films. The peaks due to Nb, O, N, and C present in the samples are indicated. The C 1*s* peak is due to the adventitious carbon present on the sample surface, and it is due to sample handling.

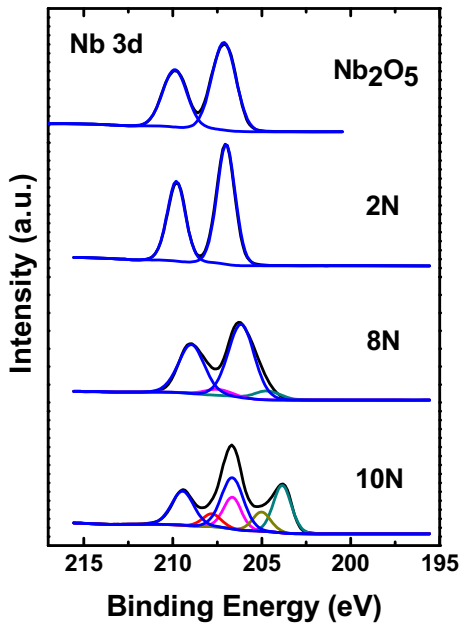

Fig. 3. Nb 3*d* core-level XPS data of Nb-O-N films. The evolution of the peak with increasing nitrogen content can be noted.

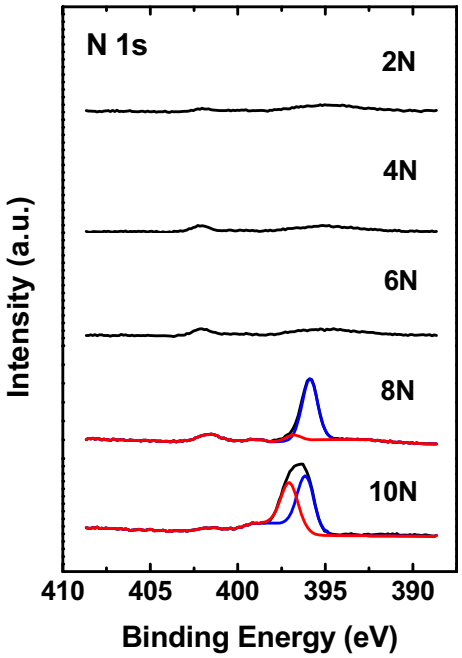

Fig. 4. Nitrogen 1*s* core-level XPS data of Nb-O-N films. The evolution of the peak with increasing nitrogen content can be noted. The absence of this peak for Nb-O-N samples deposited at lower nitrogen gas flow rates indicate that the nitrogen incorporation takes place only at certain conditions.

energies of 205.5 eV and 208.4 eV, respectively. The BE of the low binding energy component is analogous to Nb-N bond formation, resulting in a binding energy shift of − 1.6 eV. It is important to note that these lower BE components evolve while peaks corresponding to Nb_2O_5 are still evident. This is a clear indication of the fact that once nitrogen starts reacting with effective incorporation into the resulting sample, a mixture of Nb-O and Nb-N bonds exists, which is characteristic of the formation of Nb-O-N compound. Further increases in nitrogen flow rate introduce additional complexity of Nb peak resulting from a further increase in nitrogen leading to substantial chemical changes in the films. For instance, for samples deposited at a nitrogen flow rate of 10 sccm, a third component is evident at a much lower BE. For 10 sccm of nitrogen, the $3d_{5/2}$ peak is located at a lower BE of 203.9, likely corresponding to a heavily reduced Nb-O-N species approaching metallic Nb. Further evidence for such higher reduction leading to metallic nature upon nitrogen incorporation is seen in mechanical characteristics, which are discussed in subsequent sections.

The N 1*s* peak (Fig. 4) as a function of nitrogen gas flow rate also indicates the characteristic chemical bonds formation related to nitrogen in Nb-O-N films upon nitrogen incorporation. The trend observed is similar to Nb 3*d* and supports the fact that the nitrogen incorporation leading formation of Nb-O-N films is not effective until the nitrogen flow rate is ≥ 6 sccm. No peaks were observed and no

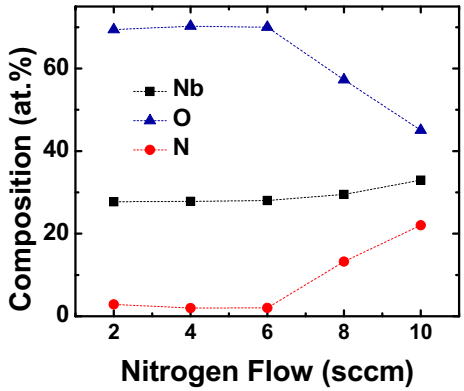

Fig. 5. Chemical composition of Nb-O-N films as a function of nitrogen gas flow rate. It is evident that the relative increase in nitrogen content balances the relative decrease in oxygen in the Nb-O-N films.

changes are seen in the N 1*s* peak region until the nitrogen flow rate is greater than 6 sccm. However, the characteristic peaks corresponding to nitrogen formation appears only when the nitrogen flow rate exceeds 6 sccm.

Corroborating with XPS analyses, Rutherford backscattering measurements (not shown) also indicate that the nitrogen incorporation is not very effective for the set of nitrogen flow rates at < 6 sccm. At higher nitrogen flow rates, an increase in the nitrogen concentration is noted confirming the formation of Nb-O-N films. Incorporation of nitrogen content in the films is accompanied by a decrease in oxygen content. Thus, the chemical composition analyses allowed for accurate determination of at.% of Nb, O, and N in the films are presented in Fig. 5. First of all, it must be emphasized that the trend observed and data confirm that the nitrogen incorporation and formation of Nb-O-N is not effective until the nitrogen flow rate is > 6 sccm. Based on the chemical analyses, the composition of the Nb-O-N films, as the nitrogen flow rate is increased, is represented by the following sequence: $NbO_{2.50} \rightarrow NbO_{2.52} \rightarrow NbO_{2.50} \rightarrow NbO_{1.94}N_{0.45} \rightarrow NbO_{1.37}N_{0.67}$. The observed chemical composition changes and formation of Nb-O-N films can be understood from thermodynamic considerations. If the heats of formation from thermo-chemical data of the respective oxide and nitride compounds of Nb are considered, it is evident that he thermal energy required for the formation of Nb_2O_5 (ΔH_f = − 1905 kJ/mol) is more favorable compared to the heats of formation for Nb-nitride compounds.[24,25,29,40]

It is anticipated that the aforementioned surface/interface chemical changes in terms of nitrogen incorporation and mixture of Nb-O and Nb-N bonds will affect the mechanical characteristics, especially the surface hardness and elastic modulus, of the Nb-O-N films. The results obtained from nano-indentation measurements are shown in Fig. 6, where variation in the hardness and elastic modulus with

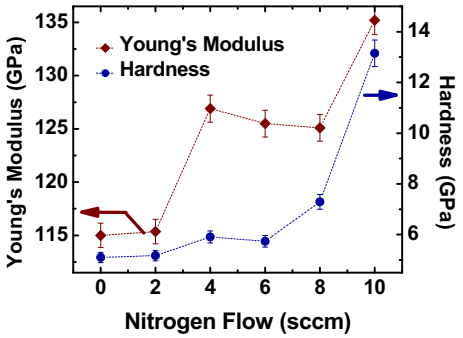

Fig. 6. Functional dependence of mechanical properties of Nb-O-N films on the nitrogen gas flow rate.

nitrogen flow rate is presented. The well-known Oliver and Pharr method[33] has been employed to calculate the mechanical characteristics; known geometry and mechanical properties of the indenter were used in the calculation. The trend in hardness and elastic modulus with increasing nitrogen flow rate in Nb-O-N films is very clear. Hardness values for Nb-O-N films ranged from ~ 5.74 GPa to 13.15 GPa, which are similar to those reported in the literature.[24,25] Additionally, the variation of hardness values with nitrogen flow rate directly correlates to the chemical changes as noted in chemical analyses. The hardness values of the Nb-O-N films deposited without any nitrogen are rather low (5 GPa to 6 GPa), which is expected since those films are ceramic, brittle Nb_2O_5. Interestingly, the hardness values stay low until the nitrogen flow rate is $>$ 6 sccm. We believe that this is due to the fact that there is no effective nitrogen incorporation and the samples are mostly Nb-oxide (Nb_2O_5) films; therefore, no net effect on the hardness of the samples is observed as there is no changes in chemical bonds. However, hardness enhancement is evident (Fig. 6) once the nitrogen incorporation is effective leading to formation of Nb-O-N films, where there is a mixture of Nb-O and Nb-N bonds as revealed by the chemical analyses. A progressive increase in nitrogen content in the films is seen to increase the hardness close to $\sim$ 16 GPa. Thus, the trend observed in hardness and elastic modulus values of the Nb-O-N films directly correlate with the chemical composition changes, i.e., nitrogen content increase in the films as a result of Nb-oxynitride formation. Note that the hardness is related to the bonding between the atoms and to the ability of the bonds to withstand deformation.[38,39] Also, nitrides exhibit the ability to withstand deformation more than the oxides. Therefore, the observed increase in hardness values must be due to the formation of Nb-oxynitride films, where the nitrogen-incorporation induced Nb-N bonds are effective in promoting the mechanical characteristics of Nb-O-N films. Similar to hardness values, elastic modulus values also exhibit the similar trend. However, the elastic modulus values increase slightly for intermediate range of nitrogen gas flow rate (4 to 6 sccm) and then finally attains higher values at higher nitrogen flow rates. Despite the fact that the hardness and elastic modulus values increase with increasing nitrogen flow rate due to films becoming oxynitride, the values determined for Nb-O-N films even for the highest flow rate employed in this work are significantly lower compared to traditional values of the nitrides. In particular, the relatively low hardness values may be due to the amorphous structure of the Nb-O-N films. Note that the GIXRD analyses indicate that all the Nb-O-N films produced are amorphous in the entire range of nitrogen flow rates. As reported by several authors and widely accepted in the literature, mechanical properties decrease when the film exhibits an amorphous structure and also when the internal stresses in the films become relaxed.[38,39] For instance, as demonstrated by Dubey et al., the magnitudes of hardness and Young's modulus are directly related to the structure. In their work, it was shown that the hardness and elastic modulus decreases when the film becomes amorphous because of the lack of hindrance to dislocation movements that grain growth tends to promote.[39]

CONCLUSION

Amorphous Nb-O-N thin films were deposited with the use of DC sputtering by varying the ratio of reactive gases while maintaining a flow rate of 10 sccm and keeping the total gas flow at 30 sccm. Chemical analyses revealed that no significant nitrogen incorporation occurs in Nb-O-N films for reactive nitrogen gas flow rates $\leq$ 6 sccm. Beyond a nitrogen flow rate of 6 sccm, the electronic structure of the films was modified with the existence of both Nb-O and Nb-N bonds leading to the formation of Nb-O-N films. Mechanical characterization showed a strong dependence on the nitrogen content and/or Nb-N bonds in the Nb-O-N films. Hardness and elastic modulus of Nb-O-N films was determined to be the highest ($\sim$ 13.15 GPa) for Nb-O-N films with highest nitrogen content. The results demonstrate a soft-to-hard transition in the mechanical behavior of Nb-O-N films, where the hardness and elastic modulus becomes substantially higher when nitrogen content in the films dominate. Such films may be useful to design antireflection coatings and functional component layers in solar cells on flexible substrates.

ACKNOWLEDGEMENT

The authors acknowledge, with pleasure, support from the National Science Foundation (NSF) with NSF-PREM Grant #DMR-1827745.

REFERENCES

1. Z. Dai, H. Dai, Y. Zhou, D. Liu, G. Duan, W. Cai, and Y. Li, *Adv. Mater. Interf.* 2, 1500167 (2015).
2. M. Serenyi, T. Lohner, P. Petrik, Z. Zolnai, Z.E. Horvath, and N.Q. Khanh, *Thin Solid Films* 516, 8096 (2008).
3. J. Wei, X. Li, H. Xue, J. Shao, R. Zhu, and H. Pang, *Adv. Mater. Interf.* 9, 1701509 (2018).

4. M.E. Gimon-Kinsel and K.J. Balkus, *Microporous Mesoporous Mater.* 28, 113 (1999).
5. J. Xia, N. Masaki, K. Jiang, and S. Yanagida, *J. Photochem. Photobiol. A Chem.* 188, 120 (2007).
6. M. Mazur, M. Szymanska, D. Kaczmarek, M. Kalisz, D. Wojcieszak, J. Domaradzki, and F. Placido, *Appl. Surf. Sci.* 301, 63 (2014).
7. T. Maruyama and S. Arai, *Appl. Phys. Lett.* 63, 869 (1993).
8. N. Ozer, M.D. Rubin, and C.M. Lampert, *Sol. Energy Mater. Sol. Cells* 40, 285 (1996).
9. K. Yoshimura, T. Miki, S. Iwama, and S. Tanemura, *Thin Solid Films* 281–282, 235 (1996).
10. E. Pehlivan, F.Z. Tepehan, and G.G. Tepehan, *Sol. Energy Mater. Sol. Cells* 87, 317 (2005).
11. K.S. Havey, J.S. Zabinski, and S.D. Walck, *Thin Solid Films* 303, 238 (1997).
12. M. Fenker, M. Balzer, R. Büchi, H. Jehn, H. Kappl, and J.-J. Lee, *Surf. Coat. Technol.* 163–164, 169 (2003).
13. J.P. Manaud, A. Poulon, S. Gomez, and Y. Le Petitcorps, *Surf. Coat. Technol.* 202, 222 (2007).
14. J.J. Olaya, L. Huerta, S.E. Rodil, and R. Escamilla, *Thin Solid Films* 516, 8768 (2008).
15. R.P. Frankenthal, *J. Electrochem. Soc.* 130, 2056 (1983).
16. P.K. Gallagher, *J. Electrochem. Soc.* 130, 2054 (1983).
17. J. Probst, U. Gbureck, and R. Thull, *Surf. Coat. Technol.* 148, 226 (2001).
18. V.A. Matylitskaya, W. Bock, K. Thoma, and B.O. Kolbesen, *Appl. Surf. Sci.* 252, 205 (2005).
19. D. Bekermann, D. Barreca, A. Gasparotto, H.W. Becker, R.A. Fischer, and A. Devi, *Surf. Coat. Technol.* 204, 404 (2009).
20. F.V. Richard, F.S. Hickernell, F.Y. Cho, 4701008 (1987).
21. V. Schwartz and S.T. Oyama, *Chem. Mater.* 9, 3052 (1997).
22. R. Brayner and G. Djéga-Mariadassou, *Catal. Today* 57, 225 (2007).
23. T. Savisalo, D.B. Lewis, and P.E. Hovsepian, *Surf. Coat. Technol.* 200, 2731 (2006).
24. M. Fenker, H. Kappl, K. Petrikowski, and R. Bretzler, *Surf. Coat. Technol.* 200, 1356 (2005).
25. M. Fenker, H. Kappl, P. Carvalho, and F. Vaz, *Thin Solid Films* 519, 2457 (2011).
26. M. Fenker, M. Balzer, and H. Kappl, *Thin Solid Films* 515, 27 (2006).
27. M. Fenker, H. Kappl, and C.S. Sandu, *Surf. Coat. Technol.* 202, 2358 (2008).
28. J.M. Chappe, P. Carvalho, S. Lanceros-Mendez, M.I. Vasilevskiy, F. Vaz, A.V. Machado, M. Fenker, H. Kappl, N.M.G. Parreira, A. Cavaleiro, and E. Alves, *Surf. Coat. Technol.* 202, 2363 (2008).
29. J.M. Chappe, P. Carvalho, A.V. Machado, F. Vaz, E. Alves, N.P. Barradas, M. Fenker, and H. Kappl, *Phys. Res. Sect. B* 266, 4927 (2008).
30. M. Fenker, H. Kappl, O. Banakh, N. Martin, and J.F. Pierson, *Surf. Coat. Technol.* 201, 4152 (2006).
31. N.R. Murphy, A.J. Moreno-Tarango, C.V. Ramana, L. Sun, J.G. Jones, and J.T. Grant, *J. Alloys Compd.* 681, 350 (2016).
32. N. Fairley, *Casa Software Ltd.*, 1999–2011.
33. W.C. Oliver and G.M. Pharr, *J. Mater. Res.* 7, 1564 (1992).
34. G. Martinez and C.V. Ramana, *Adv. Eng. Mater.* 19, 1700354 (2017).
35. A.K. Battu, S. Manandhar, and C.V. Ramana, *Adv. Mater. Interf.* 4, 1700378 (2017).
36. S.H. Mohamed and A. Anders, *Surf. Coat. Technol.* 201, 2977 (2006).
37. M. Vargas, D.M. Lopez, N.R. Murphy, J.T. Grant, and C.V. Ramana, *Appl. Surf. Sci.* 353, 728 (2015).
38. O.R. Nunez, A.J. Moreno Tarango, N.R. Murphy, and C.V. Ramana, *J. Alloys Compd.* 683, 292 (2016).
39. P. Dubey, G.A. Lopez, G. Martinez, and C.V. Ramana, *J. Appl. Phys.* 120, 245103 (2016).
40. R. Ohnishi, M. Katayama, K. Takanabe, J. Kubota, and K. Domen, *Electrochim. Acta* 55, 5393 (2010).